Molecular Catalysis 495 (2020) 111134

Contents lists available at ScienceDirect

Molecular Catalysis

journal homepage: www.elsevier.com/locate/mcat

Enhanced stability and activity for solvent-free selective oxidation of cyclohexane over Cu_2O/CuO fabricated by facile alkali etching method

Congjia Xie, Wei Wang, Yepeng Yang, Liang Jiang*, Yongjuan Chen, Jiao He, Jiaqiang Wang*

School of Chemical Sciences & Technology, National Center for International Research on Photoelectric and Energy Materials, School of Materials and Energy, Yunnan University, Kunming 650091, China

ARTICLE INFO

Keywords:
Cu_2O/CuO composites
Cu^+/Cu^{2+} ratio
Selective oxidation of cyclohexane
Cyclohexanone
Solvent-Free conditions

ABSTRACT

The easy deactivation of cuprous oxide (Cu_2O) have significantly limited their practical applications in catalysis. Formation of composites with other semiconductors including CuO is an crucial strategy for stability improvement of Cu_2O. However, this strategy developed so far has often focused on only Cu_2O thin film systems. Herein, Cu_2O/CuO composites were fabricated via a simple alkali etching method, for the first time, to stabilize the powdered Cu_2O in liquid-phase selective oxidation of cyclohexane under solvent-free conditions. The etching method presented remarkable high dispersion of copper species and an appropriate Cu^+/Cu^{2+} ratio on catalyst surface, which leads to superior catalytic activity and stability. Hot filtration experiment confirmed that Cu_2O/CuO composite was a heterogeneous catalyst which could be reused at least five times without considerable loss of catalytic activity, whereas the pure Cu_2O suffered from severe deactivation caused by oxidative decomposition of Cu_2O and copper leaching. Moreover, the amount of Cu^+ and Cu^{2+} sites on catalyst surface are dramatically affected by the amount of alkali during etching process and the catalytic performance can be further tuned by regulating the Cu^+/Cu^{2+} ratio. The Cu_2O/CuO with a molar ratio of NaOH/Cu_2O = 1:1 exhibited the highest catalytic activity with a cyclohexane conversion of 84.3 % and cyclohexanone selectivity of 77.0 %. The present work provides a promising strategy to stabilize Cu_2O catalysts in catalytic oxidation systems.

Introduction

In recent years, copper oxides have attracted considerable attention due to its prospective application in the fields of gas sensor [1], sodium ion batteries [2], catalysis [3], and supercapacitor [4]. Among the three well-established Cu-based oxides: CuO, Cu_2O and Cu_4O_3 [5], CuO is identified as the most stable copper-oxide phases, while the crystallographic and phases of Cu_2O can be easily changed under harsh condition [6]. In particular, Cu_2O, as a p-type semiconductor, has gained considerable research attention for numerous catalytic reactions due to its tunable bandgap, earth abundancy, and excellent catalytic properties [7]. Cu_2O has been reported to act as an efficient catalyst for several selective catalytic reactions such as CO oxidation [8], formaldehyde oxidation [9], phenylacetylene oxidation [10], propylene oxidation [11] and catalytic reduction of 4-nitrophenol [12]. However, owing to its susceptible chemical stability, self-reduction or self-oxidation is unavoidable when exposed to oxidizing or reducing environment deactivation [13].

To overcome these drawbacks, various strategies such as engineering crystal facet [14], controlling particle sizes [15], and incorporation of secondary components [16] has been employed to enhance the catalytic stability of Cu_2O. Especially, a number of secondary components including carbon quantum dots (CQDs) [17], reduced graphene oxide (rGO) [18], ZIF-8 [19], semiconductors [20], and metal nanoparticles [21] have been extensively studied. Moreover, it has been demonstrated that Cu_2O/CuO nanocomposites could bring new synergistic catalytic performance, which arise from the construction of unique Cu-O interfaces [22]. In this regard, incorporation of a protective layer (CuO nanowires) was shown to be an effective approach to enhance the photoelectrochemical stability of Cu_2O film [23]. Nonetheless, the redox activities of the Cu_2O photoelectrode were also suppressed after introducing the passive outer layer of CuO [23]. Therefore, the exploration of alternative strategies in enhancing both stability and activity of Cu_2O is still highly desired. As a green and simple modification method [24], chemical etching (acid treatment or alkali treatment) has been currently paid wide attention for enhance the catalytic performance of nanoparticles, including Cu_2O nanoparticles by controlling their morphologies [25]. Surface treatment by etching might be a useful approach to stabilize Cu_2O because the etched surfaces will bring about high-activity sites for enhancing chemical

* Corresponding authors.
E-mail addresses: jiangliang@ynu.edu.cn (L. Jiang), jqwang@ynu.edu.cn (J. Wang).

https://doi.org/10.1016/j.mcat.2020.111134
Received 18 April 2020; Received in revised form 10 July 2020; Accepted 22 July 2020

activities [26]. However, the contemporary use of etching for enhanced Cu_2O stability has been largely limited to thin film systems.

The selective oxidation of cyclohexane is an extraordinary significant process in petrochemical industry since its products (cyclohexanone and cyclohexanol) are the key intermediate for industrial production of nylon-66 and nylon-6 [27]. Various copper-based catalysts (such as Cu(I) complexs [28], Cu-*Zn*-BTC MOF [29], CuCrOx [30], Cu(I)-ZSM-5 [31]) have been proved to be active for oxidation of cyclohexane. However, these catalysts offer either limited conversion (< 50 %) or low selectivity (< 60 %). Additionally, fiberglass supported Cu(I)-Cu(0) compounds has been found a remarkable deactivation in cyclohexane oxidation due to the oxidation of Cu species in the presence of H_2O_2 and O_2 [32]. On the other hand, most of cyclohexane oxidation systems are still environmentally hazardous owing to the use of large amount of organic solvents, leading to the problems of high disposal wastes and severe copper leaching [33,34]. Thus, developing an efficient and environmentally friendly heterogeneous catalyst for cyclohexane oxidation under solvent-free is highly desirable.

Herein, for the first time, we report Cu_2O/CuO composites fabricated by alkali (NaOH) etching Cu_2O sphere as efficient and stable heterogeneous catalyst for liquid-phase selective cyclohexane oxidation to cyclohexanone without any solvents. The effect of alkali concentration, reaction times, and temperature on catalytic performance of Cu_2O/CuO composites were also investigated. The samples before and after oxidation reactions were comprehensively characterized regarding catalytic stability.

Experimental

Preparation of Cu_2O

Cu_2O sphere was prepared by a wet-chemical solution method according to a reported process with some modifications [35]. 20 mL of NaOH (0.05 M) solution was dispersed in 10 mL of $Cu(NO_3)_2$ (0.01 M) solution under stirring with a copper hydroxide suspension formed, and 6 mL glucose (0.1 M) solution was added dropwise into the above mixture. Subsequently, 4 mL of Na_2SO_3 (0.02 M) solution was added into the mixture under vigorous stirring. The reaction was stopped after 2 h stirring and aged for 100 min. Finally, the Cu_2O samples were obtained from centrifugation (8000 rpm, 10 min), washing with ultrapure water, and drying (80 °C, 6 h) in vacuum.

Preparation of Cu_2O/CuO composites and CuO

We refer to some previous studies and provide a facile synthesis procedure for Cu_2O/CuO here [36]. Cu_2O/CuO composites were prepared by treating 0.5 g Cu_2O with alkali (NaOH) solution with a molar ratio of NaOH: Cu_2O = 1:4, 1:2, 1:1, 2:1, respectively. The mixture was stirred constantly and kept at room temperature (25 °C) for 24 h. The solution gradually turned black, implying the Cu_2O/CuO composites were obtained. The Cu_2O/CuO composites were centrifuged, washed and finally dried (70 °C, 6 h) in vacuum. The samples synthesized via etching Cu_2O with different ratios of NaOH/Cu_2O: 1:4, 1:2, 1:1, and 2:1 were designated as Cu_2O/CuO-E (1–4), respectively. For comparison, 0.5 g Cu_2O was impregnated in 50 mL NaOH solution with a molar ratio of NaOH: Cu_2O = 50:1 for 4 days to obtain pure CuO. The CuO were centrifuged, washed and finally dried (70 °C, 6 h) in vacuum.

Catalytic oxidation of cyclohexane

Typically, cyclohexane (1 mL, 9.27 mmol), catalyst (20 mg) and oxidant tert-butyl hydroperoxide (TBHP, 3 mL) were introduced into a round-bottom flask (50 mL) connected with a condenser with magnetic stirring at 343 K for 18 h. When the reaction completed and cooled down, the catalyst were separated via filtration. The products were quantified using gas chromatography (GC, Shimadzu GC-2014, Japan) equipped with a flame ionization detector (FID) and AE.OV-624 column (30 m × 0.25 mm × 0.5 μm).

Recyclability tests and thermal filtration experiments

Thermal filtration experiments were carried out based on a modified process [37]. 3 mL cyclohexane, 0.1 g catalyst, and 3 mL TBHP was stirred at 373 K for 1 h, then the catalysts were quickly filtrated off and the filtration was further reacted with cyclohexane. For the recyclability tests, the catalysts after finishing reaction were filtrated, washed with ultrapure water and ethanol, dried in vacuum (70 °C, 5 h), and then was employed in the next tests. In order to check the leaching of copper species, copper content of the fresh and recovered catalysts were determined by ICP-MS analyzer (Agilent 7700x, USA). To confirm the structural stability of catalysts, the recovered catalysts were further examined by XRD and XPS for comparison with the fresh catalyst.

Results and discussion

Synthesis and structural characterization

The Cu_2O spheres were synthesized by a wet-chemical solution method, and the Cu_2O/CuO composites were eventually generated after etching process at the room temperature. Initially, $Cu(NO_3)_2$ was decomposed and reduced by glucose and Na_2SO_3 at room temperature to fabricate the Cu_2O spheres. After separation and drying, the Cu_2O spheres were etched by alkali solution. The final chemical composition and crystal structure of copper oxide can be adjusted by tuning the molar ratio of NaOH/Cu_2O (i.e. the concentration of NaOH), which were described in the experimental section. As demonstrated in Scheme 1, this procedure can be explained by the process of dissolution and precipitation [38] where the unique structures were ascribed to the synergetic effect of oxidation and etching. Oxygen behaves as an oxidant owing to the reaction was run and expose in air. By the addition of NaOH, the surface of Cu_2O sphere will be firstly oxidized and transformed into $Cu(OH)_2$. A strong alkali concentration further results in generation of tetrahydroxo-cuprate(II) anions with Jahn-Teller stabilization and finally production of stable CuO precipitates. It can be concluded that alkali concentrations are responsible for chemical compositions of particles and reaction kinetics. The mechanism of oxidation etching can be summarized as following equations [38]:

$$2Cu_2O + O_2 + 4H_2O = 4Cu(OH)_2 \quad (1)$$

$$Cu(OH)_2 + 2OH^- = [Cu(OH)_4]^{2-} \quad (2)$$

$$[Cu(OH)_4]^{2-} = CuO + 2OH\text{-} + H_2O \quad (3)$$

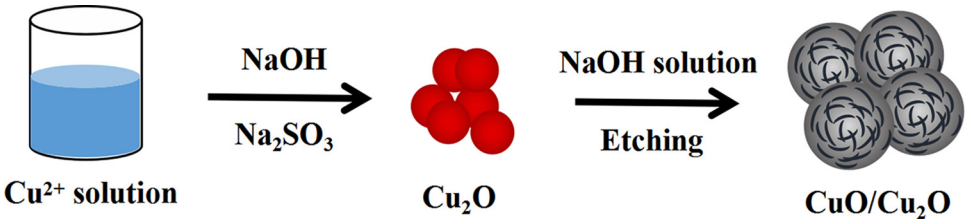

Scheme 1. Schematic illustration of the formation of Cu_2O/CuO composites.

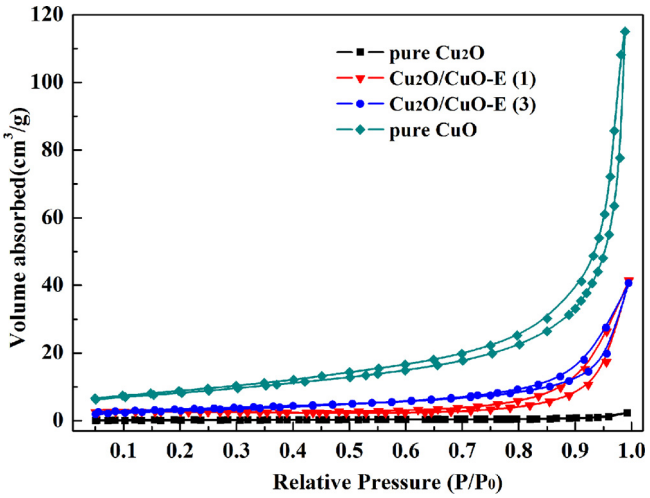

Fig. 1. N_2 sorption isotherm of pure Cu_2O, pure CuO, Cu_2O/CuO-E (1) and Cu_2O/CuO-E (3).

The N_2 adsorption-desorption isotherms of unetched Cu_2O and Cu_2O/CuO composites prepared by etching in different concentration of NaOH solution are displayed in Figs. 1 and S1. All samples exhibited the characteristic features of type IV isotherm with H1 hysteresis loops according to IUPAC classification. The corresponding BJH pore size distributions (Fig. S2) reveals the presence of the mesoporous in composites. Both the pore size and the pore size distribution range of Cu_2O/CuO samples were larger than that of unetched Cu_2O and they declined first and then increased with increasing the NaOH concentration. In addition, the textural properties of all as-prepared catalysts were summarized in Table 1. A larger BET surface area and pore volume is observed for all Cu_2O/CuO composites in relation to the pure Cu_2O ($0.8\ m^2\ g^{-1}$, $0.0035\ m^3\ g^{-1}$). When Cu_2O was etched in low NaOH concentration (NaOH/Cu_2O molar ratio of 1/2), the surface area decreases to $7.1\ m^2\ g^{-1}$ and the pore volume of the sample decreased to $0.049\ m^3\ g^{-1}$. The further raising alkali concentration (NaOH/Cu_2O molar ratio of 2) results in an increase in the BET surface area and pore volume to $12.5\ m^2\ g^{-1}$ and $0.08\ m^3\ g^{-1}$, respectively. When the sample completely transformed into CuO, it displays the highest BET surface area ($29.8\ m^2\ g^{-1}$) and pore volume ($0.17\ m^3\ g^{-1}$). This variation may be related to the decreased amount of the larger mesopores as deduced from Fig. S2 and the gradual formation of CuO nanoparticles with smaller particle size.

The crystal structure and composition of Cu_2O/CuO composites were examined and evaluated by XRD measurement. As observed from Fig. 2a, the diffraction peaks of Cu_2O at 2θ values of 29.6°, 36.4°, 42.3°, 61.3°, 73.5°, 77.3° are observed, which correspond to the lattice planes of (110), (111), (200), (220), (311), (222) of cubic Cu_2O (JCPDS no. 78-2076), respectively, indicating the successful synthesis of Cu_2O in our work. For the sample of Cu_2O/CuO composites, the characteristic peaks of Cu_2O/CuO composites are correspondingly assigned to CuO (JCPDS no. 80-0076) and Cu_2O (JCPDS no. 78-2076), which revealed the simultaneous existence of monoclinic CuO phase and cubic Cu_2O phase in synthesized catalysts. No other possible phases such as Cu or Cu $(OH)_2$ were detected. These results imply that the mixed phase Cu_2O/CuO composite can be successfully obtained by etching pure Cu_2O crystal. Meanwhile, with increasing in NaOH/Cu_2O molar ratio, the

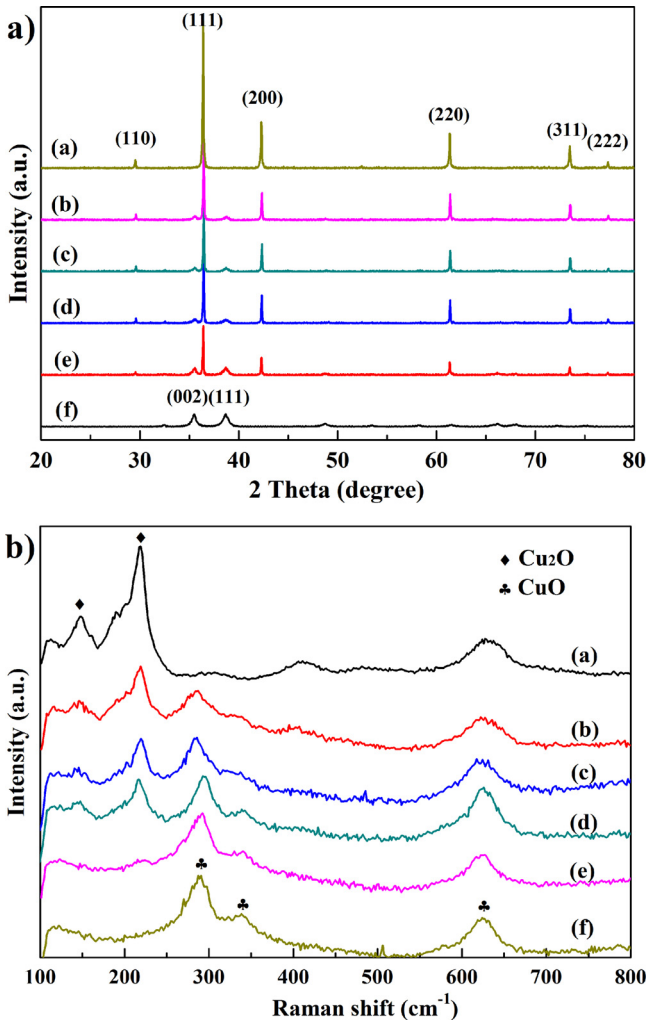

Fig. 2. a) XRD patterns and b) Raman spectra of (a) Cu_2O, (b) Cu_2O/CuO-E (1), (c) Cu_2O/CuO-E (2), (d) Cu_2O/CuO-E (3), (e) Cu_2O/CuO-E (4), (f) CuO.

Table 1
Physicochemical properties of the Cu_2O, Cu_2O/CuO composites, and CuO.

Catalyst	Weight percentage[a]		Cu^+/Cu^{2+} ratio[a]	Grain size (nm)[a]		Cu content (wt%)[b]			S_{BET} ($m^2\ g^{-1}$)[c]	V_{pore} ($m^3\ g^{-1}$)[c]	d_{pore} (nm)[c]
	Cu_2O	CuO		Cu_2O	CuO	Total (Theoretical)	Total (ICP)	External (XPS)			
Cu_2O	100	0	—	> 100	—	89.4	88.4	65.7	0.8	0.0035	18.6
Cu_2O/CuO-E (1)	83.2	16.8	5.5:1	94.1	15.8	88.0	86.5	61.3	7.6	0.064	24.1
Cu_2O/CuO-E (2)	65.0	35.0	2.1:1	91.7	15.2	85.0	82.8	59.4	7.1	0.049	16.4
Cu_2O/CuO-E (3)	44.5	55.5	1:1.1	92.5	14.0	84.4	81.4	60.9	12.1	0.062	18.5
Cu_2O/CuO-E (4)	26.4	73.6	1:2.5	96.2	17.4	82.8	80.1	62.2	12.5	0.080	22.2
CuO	0	100	0	—	21.9	80.4	77.6	65.8	29.8	0.17	23.8

[a] Weight percentage of Cu_2O and CuO, Cu^+/Cu^{2+} molar ratio, and grain size of Cu_2O and CuO calculated from the XRD data.
[b] Determined by ICP-MS and XPS analysis.
[c] BET specific surface area, pore volume, and pore diameter determined by N_2 sorption isotherm.

intensity of Cu_2O (111) planes gradually decreased while the intensity of CuO (002) planes and (111) planes both increased, indicating that the Cu_2O with largely exposed (111) planes was oxidized gradually to form CuO during etching process. With a further increase in NaOH/Cu_2O ratio to 50:1 and reaction time to 4 days, all the diffraction peaks of Cu_2O were disappeared, implying that Cu_2O can be completely converted into CuO. Furthermore, the weight percentage and the grain size of CuO and Cu_2O for each sample were calculated based on the CuO (111) and Cu_2O (111) planes, respectively, and compiled in Table 1. It can be seen that the grain size of pure Cu_2O and pure CuO are much larger than that of all CuO/Cu_2O samples. With the increase of NaOH/Cu_2O molar ratio, the grain size of CuO decreases gradually from 15.8 to 14.0 nm and then increased to 17.4 nm, while the mass ratio of CuO increased from 16.8%–73.6%. For Cu_2O/CuO-E (3), the crystalline sizes of CuO and Cu_2O were 14.0 nm and 92.5 nm, respectively, and the weight percentage of CuO and Cu_2O were 55.5 % and 45.5 %, respectively. Moreover, the actual total Cu content detected by ICP-MS and the theoretical total Cu content in these samples were listed in Table 1. The external Cu contents on the surface of samples roughly calculated by XPS have also been summarized in Table 1. The actual Cu contents in all samples were similar to theoretical values with the error less than 4%, indicating that the copper species completely precipitated. The Cu content detected by ICP were higher than those detected by XPS, attributing to the number of Cu sites exposed on the sample surface was lower than the total number of Cu sites in samples. It is worth noting that the Cu content in Cu_2O/CuO composites gradually decreases with the amount of alkali increasing, mainly due to the gradually formation of CuO.

The Raman spectra also confirmed the similar results about the composition of samples. The Raman spectra of pure Cu_2O, pure CuO, and Cu_2O/CuO composites were shown in Fig. 2b. In detail, these peaks are related to three modes (Ag, B1 g, and B2 g) reflecting the vibration of copper metal with oxygen. The bands at 300, 351 and 635 cm^{-1} are belonged to CuO and the bands at 151, 215 cm^{-1} are indexed to Cu_2O. Furthermore, the strength of two bands at 300 cm^{-1} and 351 cm^{-1} increases with increasing amount of alkali during synthetic process. The results indicate that the product change from Cu_2O through Cu_2O/CuO to CuO.

SEM was applied to observe the morphology evolution of Cu_2O etched in different concentrations of alkali solution. The corresponding SEM images were demonstrated in Fig. 3a-j. It was found that the Cu_2O exhibits a typical spherical in shape and the average size was estimated (~500 nm) in Fig. 3a,b. Cu_2O morphology changed from spherical structure to approximately spherical flower-like microstructures assembled by numerous nanoplates with the increase of NaOH/Cu_2O molar ratio, clearly implying the process of crystal etching and growth. Under low concentration of NaOH solution (i.e. NaOH/Cu_2O molar ratio = 1:4, Fig. 3c,d), the surface of original spherical Cu_2O with large exposed (111) planes (Fig. 3i) was firstly etched and oxidized into CuO nanoflakes and there are only some Cu_2O/CuO microstructures being produced. With the increase of proportion of alkali (Fig. 3e–h), numerous Cu_2O/CuO microstructures with nanoflakes were further formed on the surface of samples. When the molar ratio of NaOH/Cu_2O is 1:1 (Cu_2O/CuO-E (3), Fig. 3e–f), the raw material was the most uniformly etched, exhibiting the most well-distributed morphology. A further increase in the concentration of NaOH (Fig. 3I,j) results in deep etching and the formation of non-regular agglomerates.

The detailed structural analysis of Cu_2O/CuO-E (3) were further revealed by TEM. As shown in Fig. 4a–c, TEM images of the representative Cu_2O/CuO-E (3) verify the expected microstructure composed of a large quantity of nanoflakes. The enlarged HRTEM image in Fig. 4d indicates that the particles were composed of a bi-component of Cu_2O and CuO. The lattice distance of 0.301 nm and 0.246 nm are assigned to the (110) plane and (111) plane of Cu_2O, respectively, while the lattice spacing of 0.186 nm and 0.232 nm are corresponding to (200) plane and (111) plane of CuO, respectively. The particle size of CuO was estimated to be about 10 nm. The TEM results are in good consistent with those of XRD, and indicate that Cu_2O and CuO were well uniformly dispersed.

The high resolution Cu 2p and O 1s XPS spectra of Cu_2O and Cu_2O/CuO-E (3) catalysts are shown in Fig. 5. The Cu_2O species can be easily identified by its weak satellite from Cu 2p spectra in Fig. 5a. The peaks fitted at 932.4 eV and 952.2 eV are respectively assigned to Cu $2p_{3/2}$ and Cu $2p_{1/2}$, indicating that copper belongs to Cu^+. The Cu 2p spectra of Cu_2O/CuO-E (3) (Fig. 5a) shows two deconvoluted Cu $2p_{3/2}$ peaks at 932.9 and 934.2 eV, corresponding to two components of Cu_2O (Cu^+) and CuO (Cu^{2+}), respectively. It is indicated that the presence of both CuO and Cu_2O in composites. In addition, the main Cu $2p_{3/2}$ and Cu $2p_{1/2}$ for Cu^+ are shifted toward higher binding energies when compared with pure Cu_2O, attributed to the incorporation of Cu^{2+} with a higher binding energy values in compared with Cu^+ [25]. Compared with weak satellite in XPS Cu 2p spectra of Cu_2O, shake-up satellite peaks pointed at 944.8 and 963.4 eV in Cu 2p spectra of Cu_2O/CuO-E (3) were observed, which can be explained by different disparate orbital environment of CuO (3d9) and Cu_2O (3d10). There are weak satellite peaks of Cu_2O with full valence orbitals (3d10) because electrons can not migrate to the higher order bound state. While CuO having partially filled valence orbitals (3d9), the electronic migration to a higher bound state can be achieved. The results further indicate that there is an interaction between Cu_2O and CuO. The O 1s XPS spectrum in Fig. 5b shows that the two peaks of Cu_2O at 530.4 and 531.7 eV are referred to adsorbed oxygen species (Oads) and hydroxyl and carbonate species, respectively, whereas the O1 s peak of Cu_2O/CuO-E (3) is convoluted into two main peaks centered at about 530.2 and 531.6 eV,

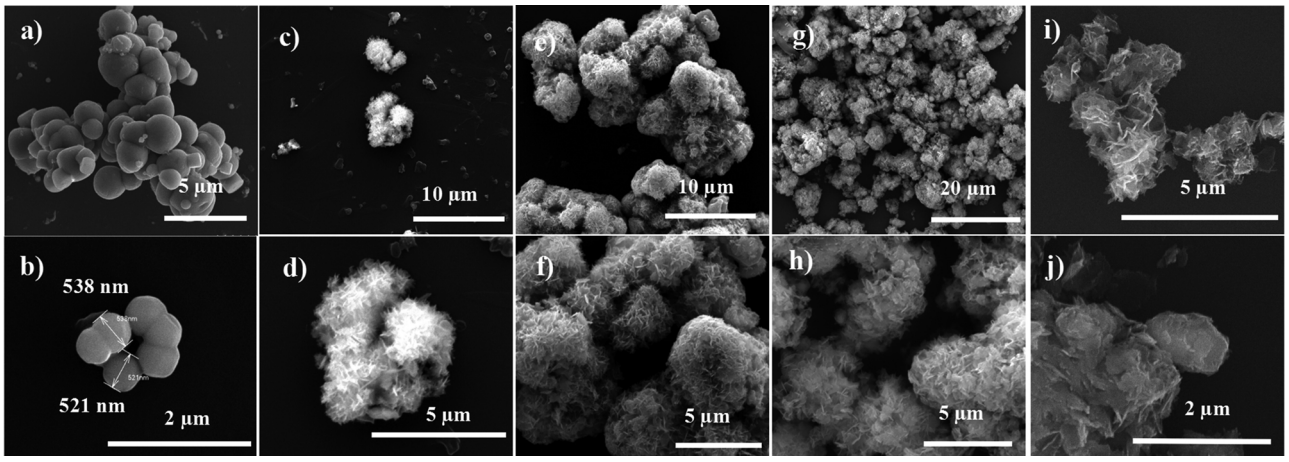

Fig. 3. SEM images of a,b) pure Cu_2O; c, d) Cu_2O/CuO-E (1); e, f) Cu_2O/CuO-E (2); g, h) Cu_2O/CuO-E (3); i, g) Cu_2O/CuO-E (4).

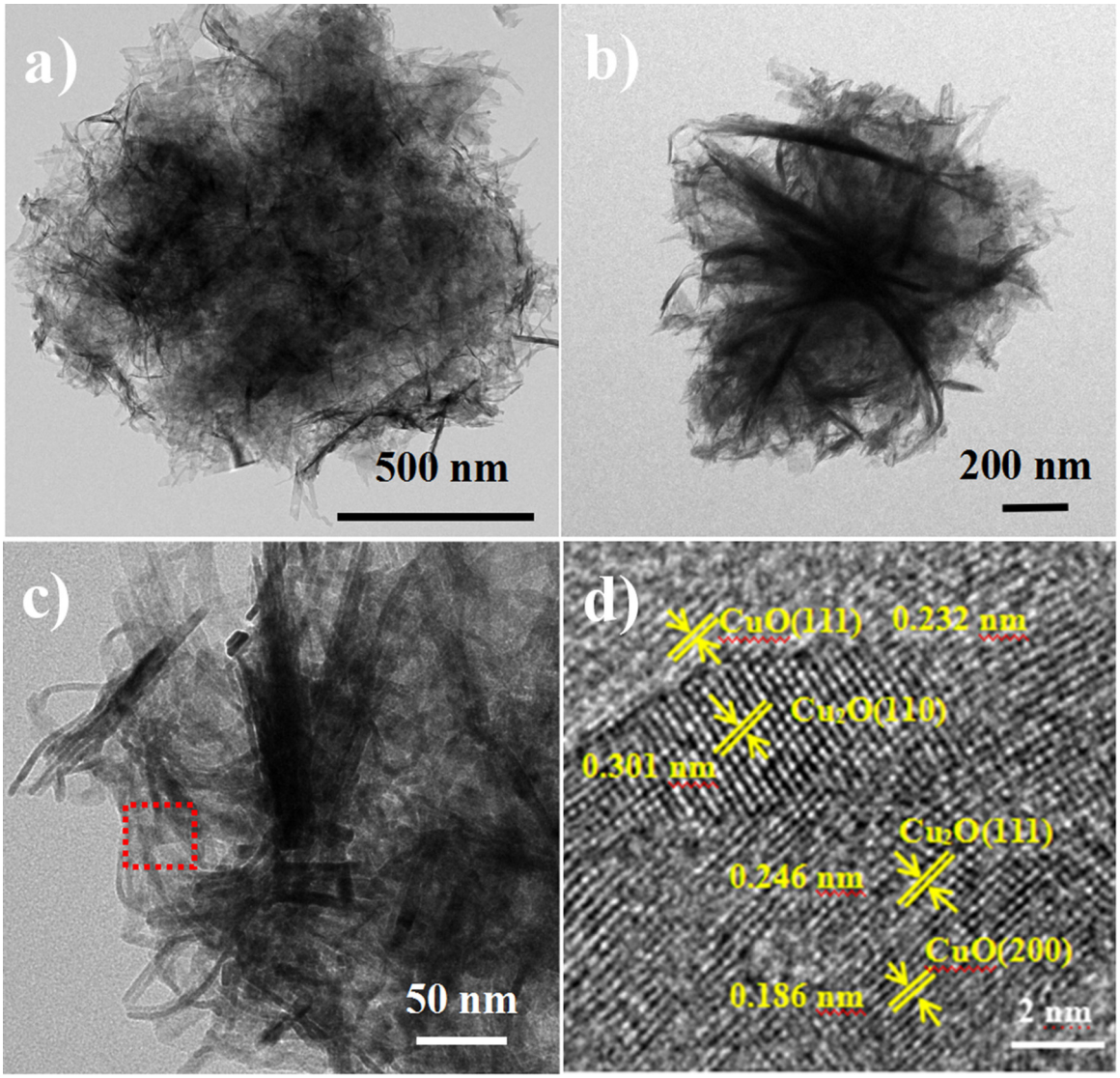

Fig. 4. a-c) TEM images and d) enlarged HRTEM of Cu_2O/CuO-E (3).

originating from surface lattice oxygen (Olatt) and adsorbed oxygen species (Oads), respectively.

Catalytic performance

The catalytic performance of the Cu_2O, CuO and Cu_2O/CuO composites for cyclohexane oxidation reaction using TBHP as oxidizer were investigated and summarized in Table 2. The blank run exhibited 24.2 % conversion of cyclohexane and negligible selectivity towards cyclohexanone (Table 2, entry 1). It can be seen that Cu_2O only obtained a 73.2 % conversion and 62.9 % selectivity towards cyclohexanone (Table 2, entry 2), which was higher than those of CuO (Table 2, entry 3). The results indicated that both Cu^+ and Cu^{2+} species were active catalytic components, yet the Cu^+ species exhibited higher catalytic activity. It is noteworthy that the catalytic performance of Cu_2O/CuO grows sharply after introducing of CuO by alkali etching Cu_2O. Meanwhile, with a further increase in proportion of CuO, a slightly decline in both conversion and selectivity was observed. Especially, the highest conversion (84.3 %) and cyclohexanone selectivity (77.0 %) were achieved over the Cu_2O/CuO-E (3) catalyst (Table 2, entry 4). To investigate the synergistic effect generated from co-existence of Cu^+ and Cu^{2+}, the turn over number (TON) of catalysts was calculated, assuming all copper (Cu^+ and Cu^{2+}) species were the active sites. Two TON numbers were defined (Table 2): TON_b referred to the total number of Cu sites detected by ICP-MS and TONs referred to the surface number of Cu sites detected by XPS [39]. All TONs values were higher than TON_b values, attributing to the number of Cu sites exposed on the sample surface was lower than the total number of Cu sites in sample. The turnover frequency (TOF) at at low conversion (< 12 %) was calculated on the basis of the number of Cu sites exposed on the sample surface detected XPS. It is found that the TON and TOF value of Cu_2O/CuO-E (3) against the catalytic oxidation of cyclohexane are the highest in comparison to other catalysts. It is well known that the presence of a porous network in a catalyst increases the contact surface area and hence enables a better diffusion of pollutants [40]. However, normalized by the BET surface areas, the specific activity of various catalysts prepared in this work show a significant difference and decrease in the order Cu_2O > Cu_2O/CuO-E (1) > Cu_2O/CuO-E (2) > Cu_2O/CuO-E (3) > Cu_2O/CuO-E (4) > CuO-E, suggesting that the surface areas are not the active site that controls the reaction rate. Generally speaking, the cyclohexane oxidation in metal oxides follows a conventional Haber-Weiss route with the major contribution from coordinatively unsaturated sites [41]. Therefore, the high surface areas of mesoporous metal oxides might not be the only reason for their good catalytic performance, and the nature of copper oxide also plays an important role.

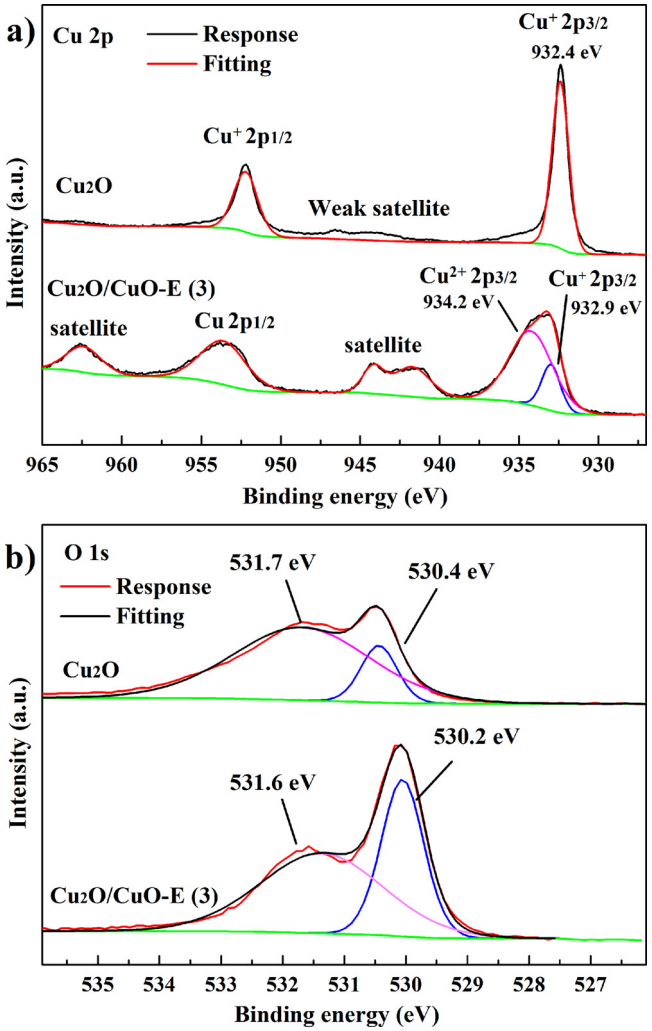

Fig. 5. XPS spectra of a) Cu 2p and b) O 1s of Cu_2O and Cu_2O/CuO-E (3).

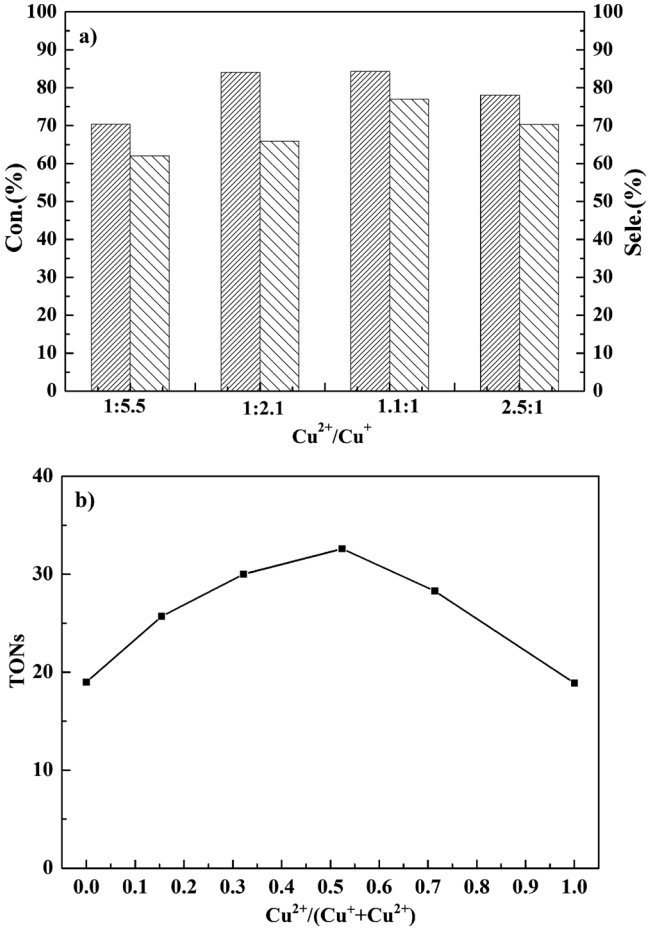

Fig. 6. a) Cyclohexane oxidation performance as a function of Cu^{2+}/Cu^{+}, b) Correlation of the TONs of cyclohexanone with $Cu^{2+}/(Cu^{+} + Cu^{2+})$.

To further gain insight into the effect of the Cu valence state on oxidation reactions, the effect of Cu^{2+}/Cu^{+} on the catalytic performance and TONs of cyclohexanone as a function of $Cu^{2+}/(Cu^{+} + Cu^{2+})$ were investigated (Fig. 6). It is notable that the TONs of

Table 2
Comparison of literature catalysts and our catalyst system for cyclohexane.[a].

Entry	Catalysts	TON_b[b]	TON_s[b]	TOF (h^{-1})[c]	Specific activity (mmol m^{-2} h^{-1})	Con. (%)[d]	Sele. (%)[e]			Yield of Cyone (%)[f]	Ref.
							Cyone	CyOH	Others		
1	Blank test	—	—	—	—	24.2	—	13.3	86.7	—	This work
2	Cu_2O	18.7	19.0	0.76	9.7	73.2	62.9	14.6	22.5	46.0	This work
3	CuO	15.5	18.9	0.94	0.3	61.4	52.4	17.1	30.5	32.2	This work
4	Cu_2O/CuO-E (1)	15.2	25.7	0.72	0.97	70.4	62.0	14.4	23.6	43.6	This work
5	Cu_2O/CuO-E (2)	23.6	32.0	0.64	0.85	84.1	65.9	13.4	20.7	55.4	This work
6	Cu_2O/CuO-E (3)	24.4	32.6	1.06	0.83	84.3	77.0	3.5	19.5	64.9	This work
7	Cu_2O/CuO-E (4)	22.0	28.3	0.69	0.54	78.1	70.3	6.7	23.0	54.9	This work
8	Cu(I) complex	—	—	—	—	47.0	73.0	27.0	—	34.3	[28]
9	Cu-Zn-BTC	—	—	—	—	40.0	51.0	49.0	—	20.4	[29]
10	Cu(I)-ZMS-5	—	—	—	—	28.0	27.7	66.0	6.3	7.6	[31]
11	CuCrOs	—	—	—	—	67.3	38.5	53.9	7.9	25.9	[42]
12	Cu-Pd/TiO_2	—	—	—	—	78.0	74.0	26.0	—	57.7	[43]

Con., conversion; Sele., selectivity.

[a] Typical reaction conditions: substrate (cyclohexane), 1 mL; catalyst, 0.02 g; cyclohexane: TBHP, 3 mL; reaction temperature, 70 °C; time, 18 h.

[b] TON_b = Moles of product yield/moles of Cu sites (ICP values) in catalyst. TON_s = Moles of product yield/moles of external Cu sites (XPS values) in catalyst.

[c] TOF = moles of product yield per mole of catalyst per hour) values under a kinetically controlled regime at 70 °C for 1 h.

[d] Cyclohexane conversion = Moles of cyclohexane reacted/initial moles of cyclohexane × 100 %.

[e] Product selectivity = Moles of this product/Moles of each product × 100 %, CyOH: cyclohexanol, Cyone: cyclohexanone, others: 2-Butanone, 3-methoxy-3-methyl and1-Pentene, 4,4-dimethyl.

[f] Yield of Cyone = Cyclohexane conversion × selectivity of Cyone/100.

cyclohexanone increased steadily at low $Cu^{2+}/(Cu^{+} + Cu^{2+})$, reached a maximum at $Cu^{2+}/(Cu^{+} + Cu^{2+}) = 0.5$, and decreased with further increases in the ratio of Cu^{2+} (Fig. 6b). Therefore, the optimal TONs of cyclohexanone on the Cu_2O/CuO-E (3) catalyst lies in the high disperse of Cu^{2+} site (Table 1) and the cooperative effect of Cu^{2+} and Cu^{+}. In addition, the excessive Cu^{2+} incorporated is unfavorable to improve the catalytic activities including conversion and selectivity to cyclohexanone. Therefore, an appropriate Cu^{+}/Cu^{2+} ratio is a determined factor for effective enhancement in catalytic properties of Cu_2O for cyclohexane oxidation. The catalytic performance of our Cu_2O/CuO composites catalysts were further compared with previous literature reports on Cu based catalysts (Table 2, entries 8–12). These results give a strong evidence that the active Cu^{+}/Cu^{2+} species play a vital role in the presence oxidation reaction. Compared with the reported Cu-based catalysts, the Cu_2O/CuO composites catalysts exhibits superior catalytic properties for cyclohexane oxidation. Consequently, the Cu_2O/CuO composite is an excellent candidate for liquid phase cyclohexane oxidation in the solvent-free system.

Influence of reaction time

The effect of the reaction time on cyclohexane oxidation over Cu_2O/CuO-E (3) was studied from 2 h–24 h and shown in Fig. 7. It is found that the increasing reaction time from 2 h to 18 h generated a continuous and considerable increase of cyclohexane conversion from 50.8%–84.3% and cyclohexanone selectivity from 22.5%–77.0%, respectively. In contrast, the selectivity towards cyclohexanol clearly decreased from 27.5 % to 3.5 %. Additionally, with further increasing reaction time, little change of cyclohexane conversion and a significant decrease of cyclohexanone selectivity from 77.0%–69.4% were observed, along with a decrease of cyclohexanol from 3.5 % to 2%. This is due to the formation of deep oxidation products.

Effect of reaction temperature

Effect of the reaction temperature on oxidation reaction of cyclohexane over Cu_2O/CuO-E (3) was investigated in the range of 30 − 70 °C. The results in Fig. 8 showed strong dependent on reaction temperature. When the reaction temperature was low (≤ 40 °C), the conversion of cyclohexane increased slightly and there was almost no target product (cyclohexanol or cyclohexanone) produced. With the reaction temperature raising from 40 to 70 °C, both substrate conversion and product (cyclohexanone) selectivity increased sharply and the maximum values are obtained at 70 °C.

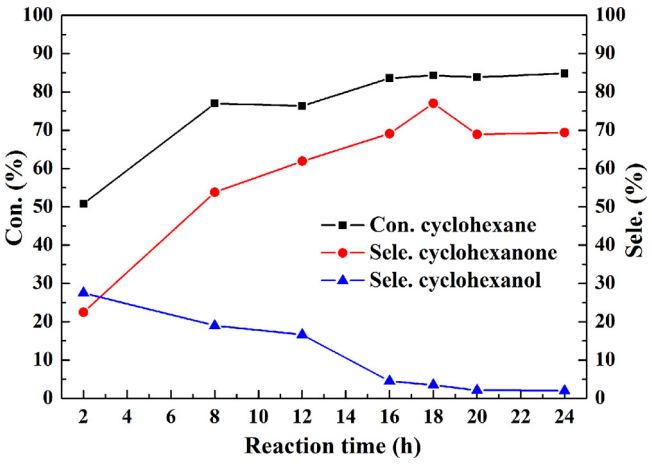

Fig. 7. Effect of reaction time on cyclohexane oxidation performance over Cu_2O/CuO-E (3).

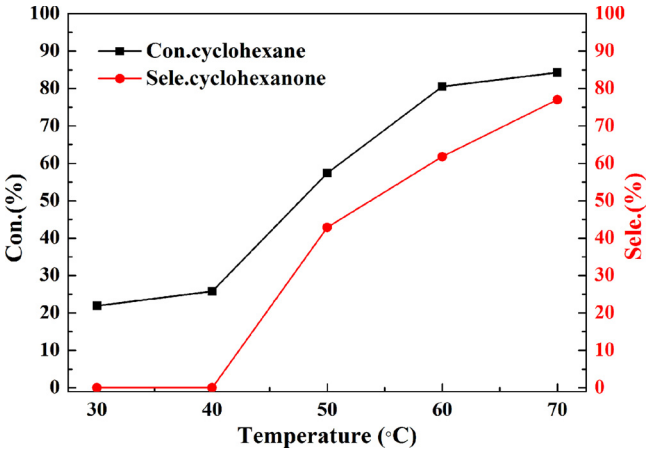

Fig. 8. Effect of reaction temperature on the oxidation of cyclohexane performance over Cu_2O/CuO-E (3).

The reusability and hot filtration experiment

To identify whether the CuO/CuO-E (3) catalyst is a heterogeneous catalyst, hot filtration testing was operated based on a modified process [37]. No further reaction of filtrate after hot filtration was detected compared to before the filtration, indicating that the active species (copper) were barely leached out and the CuO/CuO-E (3) did act as a heterogeneous catalyst.

To verify the recycling performance of pure Cu_2O and Cu_2O/CuO-E (3) catalyst, recycling test were carried out under optimized conditions (i.e. 70 °C, 18 h, cyclohexane 1 mL, TBHP 3 mL) and the results are shown in Fig. 9a,b. Notably, pure Cu_2O catalyst suffered from marked deactivation with a selectivity of the cyclohexanone decline from 68.6%–11.4% after the third run (Fig. 9b). In order to investigate the reasons for the decrease of the catalytic activity of Cu_2O, elemental analysis of the catalyst before and after reaction were investigated by ICP-MS, with the results as listed in Table 3. The Cu content in Cu_2O decreased by 20 % after the first run, suggesting that copper leaching did occur, hence, affecting the reactivity of the catalyst upon subsequent reuse. In contrast, Cu_2O/CuO composites exhibited a very high catalytic stability with no significant loss of the catalytic properties after five cycles. Accordingly, the leaching loss of Cu is less than 0.6 wt. % (Table 3), indicating that Cu active sites loss was effectively inhibited in Cu_2O/CuO-E (3) catalyst during reactions. This result was consistent with that of fast hot catalyst filtration.

In order to confirm the structural stability of the catalysts, the recycled catalysts were characterized by XRD and XPS and the results are shown in Fig. 9c–h. The XPS composition analyses of fresh and utilized samples are compiled in Table 3. Clearly, the XRD pattern of utilized Cu_2O (Fig. 9c) showed the characteristic diffraction peaks of Cu(II) carbonate dihydroxide. The Cu 2p XPS spectra of utilized Cu_2O (Fig. 9e) show that the two peaks of Cu $2p_{3/2}$ and Cu $2p_{1/2}$ located at 934.8 eV and 954.3 eV, respectively, were attributed to the Cu(II) carbonate dihydroxide. Correspondingly, the O 1s peak of utilized Cu_2O (Fig. S3) located at 532.2 eV was attributed to hydroxyl and carbonate species. According to the peaks area, the molar percentage of Cu^{+} and Cu^{2+} were calculated and listed in Table 3. It noted that a very high Cu^{2+}/Cu^{+} molar ratio of 28 on the surface of utilized Cu_2O was estimated. The results suggested that the pure Cu_2O was unstable in the reaction system and large amount of Cu_2O transformed into Cu(II) carbonate dihydroxide in the first catalytic activity test. However, The XRD patterns (Fig. 9d) and XPS spectra (Figs. 9g and S4) of the recycled Cu_2O/CuO-E (3) were similar to the fresh one, demonstrating that the Cu_2O/CuO composite has its compositions unchanged after reaction. According to Table 3, the utilized Cu_2O/CuO-E (3) possesses a relatively lower Cu^{+} content (19.0 %) compared with that in fresh catalysts (21.3

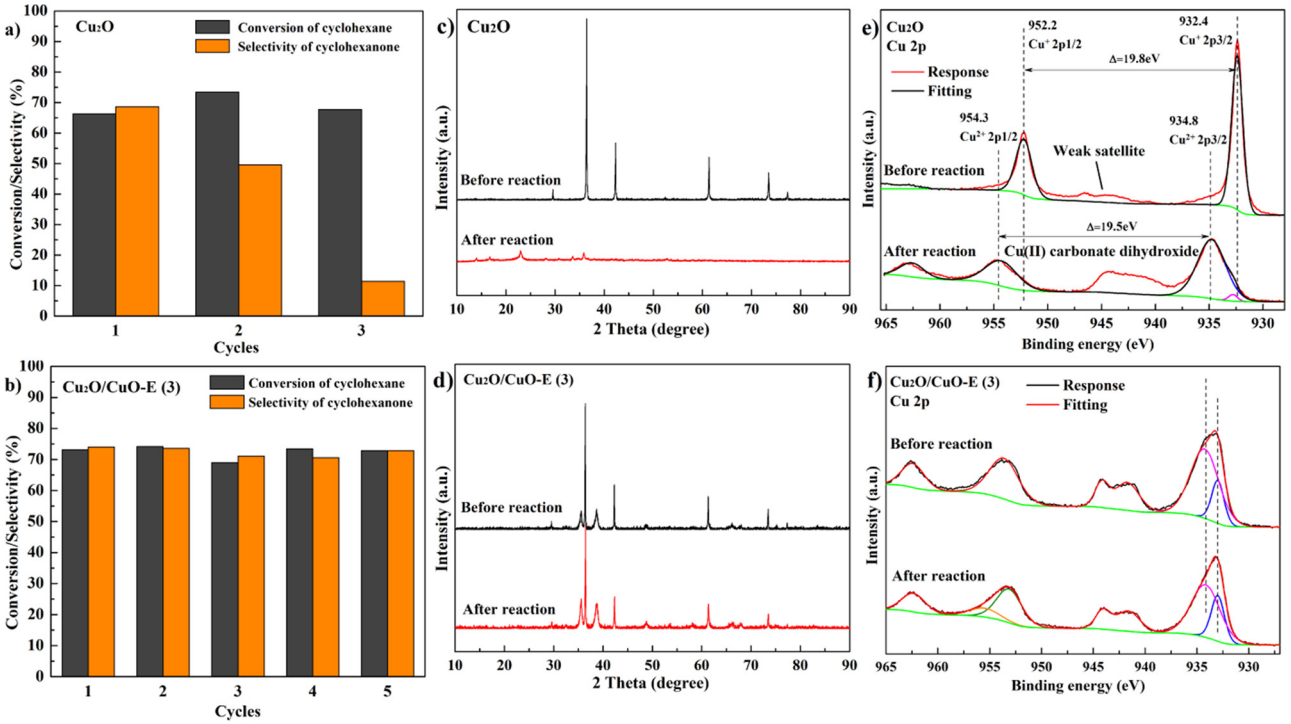

Fig. 9. Recyclability performance of a) pure Cu_2O and b) Cu_2O/CuO-E (3); c-d) XRD patterns and e-f) Cu 2p XPS spectra of catalysts (Cu_2O and Cu_2O/CuO-E (3)) before and after reaction.

%). 2% increase of Cu^{2+} content indicated that the transition from Cu^{+} to Cu^{2+} during the reaction stage can be effectively inhibited. These results indicated that the leaching of Cu species and the oxidation transformation of Cu^{+} into Cu^{2+} were responsible for the deactivation of Cu_2O during the catalytic reaction. It is also disclosed that the Cu_2O/CuO catalyst was stable and could be reused after the reaction.

The proposed reaction mechanism

A mechanistic pathway for cyclohexane oxidation over Cu_2O/CuO composites was proposed and depicted in Scheme 2. It is reported that the reaction pathway follows a free-radical chain reaction mechanism [44]. According to the Haber-Weiss cycle [41], the first step of the oxidation is an initiation step and the initiation rate strongly depends on the coordination to unsaturated metal centers [41]. For Cu_2O/CuO catalyst, the oxidant TBHP could be decomposed into active radicals $tBuO^{\cdot}$ and $tBuOO^{\cdot}$ (Eqs. (1) and (2)) in the presence of copper species (Cu^{I}/Cu^{II}). Subsequently, $tBuO^{\cdot}$ radicals can extract H from cyclohexane (Cy) to produce cyclohexyl radical ($Cy^{\cdot}$) (Eq. (4)). Afterwards, $Cy^{\cdot}$ would further interact with O_2 which could come from air atmosphere or the adsorbed oxygen on the surface of metal oxide, leading to the generation of the peroxyl radical ($CyOO^{\cdot}$). $CyOO^{\cdot}$ further performs the H-abstraction from Cy to produce CyOOH and $Cy^{\cdot}$ (Eq. (5)). Over copper (Cu^{I}/Cu^{II}) sites, the CyOOH will decompose to $CyO^{\cdot}$ and $CyOO^{\cdot}$ radicals (Eqs. (6) and (7)), in a sequence that finally yields cyclohexanol (CyOH) and cyclohexanone (Cy = O) (Eqs. (8) and (9)). Alternatively, cyclohexanone and cyclohexanol can originate from the recombination of two CyOOH (Eq. (10)). Cyclohexanol can also derive from insertion of lattice oxygen from the metal oxide to the $Cy^{\cdot}$ adsorbed over the catalyst surface [41].

Overall, according to the report by Conte et al., the catalytic performance of the metal oxides for cyclohexane oxidation mainly depends on the coordination to unsaturated metal centers, adsorbed oxygen and lattice oxygen from the metal oxides [41]. Here, owing to Cu^{I} coordinatively unsaturated sites, the oxidation reactions are initiated much faster over Cu_2O and Cu_2O/CuO in comparison to CuO, leading to the rapid production of $tBuO^{\cdot}$ radicals and decomposition of CyOOH. This results in little accumulation of CyOOH in reaction system and rapid progression all the way to CyOH (Eqs. (6) and (8)). In this regard, we believe that pure Cu_2O is more active than pure CuO for cyclohexane oxidation. This result is full agreement with the experimental results in catalytic performance.

Moreover, according to the above results and discussion, we can deduce the deactivation mechanism of Cu_2O catalysts in cyclohexane oxidation reaction (Scheme 3). The Cu^{I} catalyst is more active and effective for TBHP decomposition in initiation step. However, a higher initiation rate over Cu^{I} sites will also lead to rapid production of OH^{-}. If the consumption rate of OH^{-} is slower than its generation rate, the

Table 3
ICP and XPS composition analyses of fresh and utilized Cu_2O and Cu_2O/CuO-E (3).

Catalyst	Cu Content(μg mL^{-1})[a]	Cu molar percentage[b]		Cu^{2+}/Cu^{+} ratio[b]	O-bonding molar percentage[b]		Olatt/Oads ratio[b]
		Cu^{2+}	Cu^{+}		Olatt	Oads	
Fresh Cu_2O	236.3	0.0	100.0	0	-	-	-
Utilized Cu_2O	189.2	96.6	3.4	28:1	-	-	-
Fresh Cu_2O/CuO-E (3)	141.6	78.7	21.3	3.69:1	50.3	49.7	1:1
Utilized Cu_2O/CuO-E (3)	140.7	81.0	19.0	4.25:1	38.8	60.2	1:1.5

[a] Determined by ICP − MS analysis.
[b] Calculated by XPS analysis.

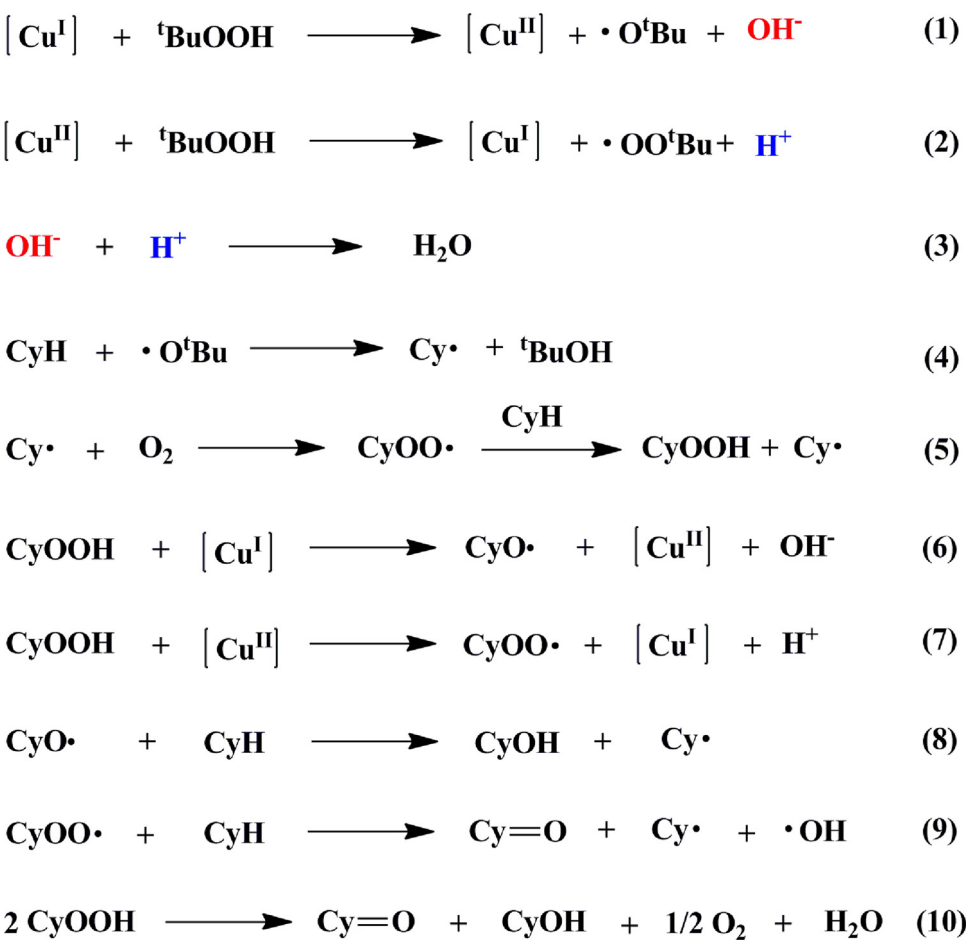

Scheme 2. Proposed reaction equations for cyclohexane oxidation with TBHP, catalyzed by Cu_2O/CuO catalyst.

excessive OH^- would further reacted with as-generated Cu^{II}, finally resulting in the formation of $Cu_2(OH)_2CO_3$ and the deactivation of Cu_2O. For Cu_2O/CuO composites, in initiation step, Cu^{II} sites in composites can also facilitate the decomposition of TBHP to give H^+ (Eq. (2)) [45]. The H^+ could not only accelerate the the deprotonation of reactant substrate (Eq. (4)) [31], but also could consume excessive OH^- generated from Eq. (1), thus avoiding generation of $Cu_2(OH)_2CO_3$ and further inhibiting the deactivation of Cu_2O. Meanwhile, the consumption of OH^- and H^+ can also promote the reaction equilibrium shifting toward the right side, leading to further accelerate the initiation rate. This synergistic effect of Cu^I and Cu^{II} is the main cause of the higher stability and catalytic performance of Cu_2O/CuO than that of pure Cu_2O and pure CuO.

Conclusions

We report a facile and promising method to stabilize Cu_2O in liquid phase cyclohexane oxidation reaction in the presence of TBHP. Cu_2O/CuO composites were successfully synthesized by mild etching of Cu_2O in NaOH solution. The as-prepared Cu_2O/CuO-E (3) achieved higher catalytic performance (84.3 % cyclohexane conversion, 77.0 % cyclohexanone selectivity) than pure Cu_2O and many reported Cu-based catalysts. Hot filtration experiment proved that the Cu_2O/CuO composites was a heterogeneous catalyst which can be reused at least five times with almost the same activity. The Cu^{2+} and Cu^+ species were found to be well distributed on the surface of catalyst, leading to an enhanced synergetic catalysis effect. An appropriate Cu^+/Cu^{2+} ratio provides a matched reaction speed on Cu_2O and CuO nanodomain, which thereby improved the catalytic performance and prevented the Cu_2O species from oxidative decomposition. The current study provide a new strategy for designing high stability Cu_2O-based catalyst with potential applications in cyclohexane oxidation.

CRediT authorship contribution statement

Congjia Xie: Conceptualization, Methodology, Writing - original draft. **Wei Wang:** Methodology, Supervision. **Yepeng Yang:** Validation, Investigation. **Liang Jiang:** Conceptualization, Writing - review & editing. **Yongjuan Chen:** Software. **Jiao He:** Resources, Supervision. **Jiaqiang Wang:** Conceptualization, Writing - review & editing.

Declaration of Competing Interest

The authors declare that they have no known competing financial interests or personal relationships that could have appeared to

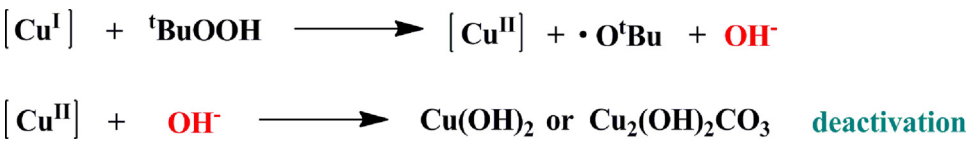

Scheme 3. Initiation step of cyclohexane oxidation over Cu_2O catalyst.

influence the work reported in this paper.

Acknowledgments

This work was supported by the National Natural Science Foundation of China (21573193) and Key Research and Development Plan of Yunnan Province (2018BA065). The authors also thank the Industrialization Cultivation Project (2016CYH04) from Yunnan Provincial Department of Education, Yunling Scholars of "Ten Thousand Talents Program" of Yunnan Province, the Program for Innovation Team of Yunnan Province, and Yunnan Provincial Collaborative Innovation Center of Green Chemistry for Lignite Energy for financial support. The authors also thank the Program for Science and Technology Projects of Kunming (2019-1-N-25318000002603) for financial support.

Appendix A. Supplementary data

Supplementary material related to this article can be found, in the online version, at doi:https://doi.org/10.1016/j.mcat.2020.111134.

References

[1] Z.K. Xu, Y.Y. Luo, G.T. Duan, Self-Assembly of Cu_2O Monolayer Colloidal Particle Film Allows the Fabrication of CuO Sensor with Superselectivity for Hydrogen Sulfide, ACS Appl. Mater. Interfaces 11 (2019) 8164–8174.
[2] X.J. Zhang, W. Qin, D.S. Li, D. Yan, B.W. Hu, Z. Sun, L.K. Pan, Metal–organic framework derived porous CuO/Cu_2O composite hollow octahedrons as high performance anode materials for sodium ion batteries, Chem. Commun. 51 (2015) 16413–16416.
[3] D.H. Jiang, J.B. Xue, L.Q. Wu, W. Zhou, Y.G. Zhang, X.H. Li, Photocatalytic performance enhancement of CuO/Cu_2O heterostructures for photodegradation of organic dyes: Effects of CuO morphology, Appl. Catal. B: Environ. 211 (2017) 199–204.
[4] J.J. Ruan, Y.Q. Huo, B. Hu, Three-dimensional $Ni(OH)_2$/Cu_2O/CuO porous cluster grown on nickel foam for high performance supercapacitor, Electrochim. Acta 215 (2016) 108–113.
[5] D.S. Murali, S. Aryasomayajula, Thermal conversion of Cu_4O_3 into CuO and Cu_2O and the electrical properties of magnetron sputtered Cu_4O_3 thin films, Appl. Phys. A 124 (2018) 124–279.
[6] J. Ghijsen, Lv. Tjeng, J. Van Elp, H. Eskes, J. Westerink, G. Sawatzky, M. Czyzyk, Electronic structure of Cu_2O and CuO, Phys. Rev. B 38 (1988) 11322.
[7] A.M. Harzandi, J.N. Tiwari, H.S. Lee, H. Jeon, W.J. Cho, G. Lee, J. Baik, J.H. Kwak, K.S. Kim, Efficient CO Oxidation by 50-Facet Cu_2O Nanocrystals Coated with CuO Nanoparticles, ACS Appl. Mater. Interfaces 9 (2017) 2495–2499.
[8] Z.H. Zhang, H. Wu, Z.Y. Yu, R. Song, K. Qian, X.Y. Chen, J. Tian, W.H. Zhang, W.X. Huang, Site-resolved Cu_2O catalysis in the oxidation of CO, Angew. Chem. Int. Ed. 58 (2019) 4276–4280.
[9] S. Momeni, F. Sedaghati, CuO/Cu_2O nanoparticles: A simple and green synthesis, characterization and their electrocatalytic performance toward formaldehyde oxidation, Microchem. J. 143 (2018) 64–71.
[10] L.L. Li, C.Y. Nan, Q. Peng, Y.D. Li, Selective Synthesis of Cu_2O Nanocrystals as Shape-Dependent Catalysts for Oxidative Arylation of Phenylacetylene, Chem. Eur. J. 18 (2012) 10491–10496.
[11] B. Reitz John, I. Solomon Edward, Propylene oxidation on copper oxide surfaces: electronic and geometric contributions to reactivity and selectivity, J. Am. Chem. Soc. 120 (1998) 11467–11478.
[12] Y.H. Wu, M.T. Song, Q.J. Wang, T. Wang, X.J. Wang, A highly selective conversion of toxic nitrobenzene to nontoxic aminobenzene by Cu_2O/Bi_2MoO_6, Dalton Trans. 47 (2018) 8794–8800.
[13] L. Zhao, L.P. Kong, C.Z. Liu, Y.Y. Wang, L.Y. Dai, AgCu/SiC-powder: A highly stable and active catalyst for gas-phase selective oxidation of alcohols, Catal. Commun. 10 (2017) 1–4.
[14] Y. Kwon, A. Soon, H. Han, H. Lee, Shape effects of cuprous oxide particles on stability in water and photocatalytic water splitting, J. Mater. Chem. A. 3 (2015) 156–162.
[15] G. Wang, R. van den Berg, C.D. Donega, K.P. de Jong, P.E. de Jongh, Silica-supported Cu_2O nanoparticles with tunable size for sustainablehydrogen generation, Appl. Catal. B: Environ. 192 (2016) 199–207.
[16] C.Y. Toe, J. Scott, R. Amal, Y.H. Ng, Recent advances in suppressing the photocorrosion of cuprous oxide for photocatalytic and photoelectrochemical energy conversion, J. Photochem. Photobiol. C. (40) (2019) 191–211.
[17] H.T. Li, Y.D. Deng, Y.D. Liu, X. Zeng, D. Wiley, J. Huang, Carbon quantum dots and carbon layer double protected cuprous oxide for efficient visible light CO_2 reduction, Chem. Commun. (Camb.) 55 (2019) 4419–4422.
[18] S.Y. Gong, J.Y. Chen, X.F. Wu, N. Han, Y.F. Chen, In-situ synthesis of Cu_2O/reduced graphene oxide composite as effective catalyst for ozone decomposition, Catal. Commun. 106 (2018) 25–29.
[19] B. Li, J.G. Ma, P. Cheng, Silica-Protection-Assisted Encapsulation of Cu_2O Nanocubes into a Metal-Organic Framework (ZIF-8) To Provide a Composite Catalyst, Angew. Chem. Int. Ed. 57 (2018) 6834–6837.
[20] X. Xu, Z.H. Gao, Z.D. Cui, Y.Q. Liang, Z.Y. Li, S.L. Zhu, X.J. Yang, J.M. Ma, Synthesis of Cu_2O Octadecahedron/TiO_2 Quantum Dot Heterojunctions with High Visible Light Photocatalytic Activity and High Stability, ACS Appl. Mater. Interfaces 8 (2016) 91–101.
[21] L.P. Han, L. Zhang, G.F. Zhao, Y.F. Chen, Q.F. Zhang, R.J. Chai, Y. Liu, Y. Lu, Copper-Fiber-Structured Pd-Au-CuOx, Preparation and catalytic performance in the vapor-phase hydrogenation of dimethyl oxalate to ethylene glycol, ChemCatChem 8 (2016) 1065–1073.
[22] S.D. Sun, X. Zhang, J. Cui, Q. Yang, S.H. Liang, Tuning interfacial Cu-O atomic structures for enhanced catalytic applications, Chem. Asian J. 14 (2019) 2912–2924.
[23] P. Wang, Y.H. Ng, R. Amal, Embedment of anodized p-type Cu_2O thin films with CuO nanowires for improvement in photoelectrochemical stability, Nanoscale 5 (2013) 2952–2958.
[24] L. Han, X.Y. Yu, X.W. Lou, Formation of Prussian-Blue-Analog Nanocages via a Direct Etching Method and their Conversion into Ni–Co-Mixed Oxide for Enhanced Oxygen Evolution, Adv. Mater. 28 (2016) 4601–4605.
[25] D. Choi, D.J. Jang, Facile fabrication of CuO/Cu_2O composites with high catalytic performances, New J. Chem. 41 (2017) 2964–2972.
[26] F. Amano, T. Ebina, B. Ohtani, Enhancement of photocathodic stability of p-type copper(I) oxide electrodes by surface etching treatment, Thin Solid Films 550 (2014) 340–346.
[27] R.H. Liu, H. Huang, H.T. Li, Y. Liu, J. Zhong, Y.Y. Li, S. Zhang, Z.H. Kang, Metal Nanoparticle/Carbon Quantum Dot Composite as a Photocatalyst for High-Efficiency Cyclohexane Oxidation, ACS Catal. 4 (2014) 328–336.
[28] F. Farzaneh, F. Moghzi, Investigation of the catalytic behavior of a Cu coordination polymer capped polyoxometalate as an oxidation catalyst, Reac. Kinet. Mech. Cat. 115 (2015) 175–185.
[29] A.M.P. Peedikakkal, A.A. Jimoh, M.N. Shaikh, B.E. Ali, Mixed-metal metal–Organic frameworks as catalysts for liquid-phase oxidation of toluene and cycloalkanes, Arab. J. Sci. Eng. 42 (2017) 4383–4390.
[30] S.S. Acharyya, S. Ghosh, S. Adak, D. Tripathi, R. Bal, Fabrication of $CuCr_2O_4$ spinel nanoparticles: a potential catalyst for the selective oxidation of cycloalkanes via activation of C_{sp3}-H bond, Catal. Commun. 59 (2015) 145–150.
[31] X.X. Zhou, H.R. Chen, X.Z. Cui, Z.L. Hua, Y. Chen, Y. Zhu, Y.D. Song, Y. Gong, J.L. Shi, A facile one-pot synthesis of hierarchically porous Cu(I)-ZSM-5 for radicals-involved oxidation of cyclohexane, Appl. Catal. A Gen. 451 (2013) 112–119.
[32] T.A. Balandina, T.Y. Larina, N.I. Kuznetsova, B.S. Balzhinimaev, Copper catalysts based on fiberglass supports for hydrocarbon oxidation reactions with the participation of hydrogen peroxide, React. Kinet. Catal. Lett. 49 (2008) 499–505.
[33] S. Rana, S.B. Jonnalagadda, CuO/Graphene Oxide Nanocomposite as Highly Active and Durable Catalyst for Selective Oxidation of Cyclohexane, ChemistrySelect 2 (2017) 2277–2281.
[34] H. Sand, R. Weberskirch, Bipyridine copper functionalized polymer resins as support materials for the aerobic oxidation of alcohols, Polym. Int. 66 (2017) 428–435.
[35] Y.B. Du, C.G. Niu, L. Zhang, M. Ruan, X.J. Wen, X.G. Zhang, G.M. Zeng, Synthesis of Ag/AgCl hollow spheres based on the Cu_2O nanospheres as template and their excellent photocatalytic property, Mol. Catal. 436 (2017) 100–110.
[36] L. Zhang, Z.M. Cui, Q. Wu, D. Guo, Y. Xu, L. Guo, Cu_2O-CuO composite microframes with well-designed micro/nano structures fabricated via controllable etching of Cu_2O microcubes for CO gas sensors, CrystEngComm 15 (2013) 7462–7467.
[37] X.C. Liu, J. He, L.J. Yang, Y.N. Wang, S.H. Zhang, W. Wang, J.Q. Wang, Liquid-phase oxidation of cyclohexane to cyclohexanone over cobalt-doped SBA-3, Catal. Commun. 11 (2010) 710–714.
[38] J.C. Park, J. Kim, H. Kwon, H. Song, Gram-Scale Synthesis of Cu_2O Nanocubes and Subsequent Oxidation to CuO Hollow Nanostructures for Lithium-Ion Battery Anode Materials, Adv. Mater. 21 (2009) 803–807.
[39] W.J. Zhou, R. Wischert, K. Xue, Y.T. Zheng, B. Albela, L. Bonneviot, J.M. Clacens, F.D. Campo, M. Pera-Titus, P. Wu, Highly Selective Liquid-Phase Oxidation of Cyclohexane to KA Oil over Ti-MWW Catalyst: Evidence of Formation of Oxyl Radicals, ACS Catal. 4 (2014) 53–62.
[40] J.L. Wang, J.G. Li, C.J. Jiang, P. Zhou, P.Y. Zhang, J.G. Yu, The effect of manganese vacancy in birnessite-type MnO_2 on room-temperature oxidation of formaldehyde in air, Appl. Catal. B: Environ. 204 (2017) 147–155.
[41] M. Conte, V. Chechik, Spin trapping of radical intermediates in gas phase catalysis: cyclohexane oxidation over metal oxides, Chem. Commun. 46 (2010) 3991–3993.
[42] L. Sun, J.H. Liu, W. Luo, Y. Yang, F. Wang, C. Weerakkody, S.L. Sui, Preparation of amorphous copper-chromium oxides catalysts for selective oxidation of cyclohexane, Mol. Catal. 460 (2018) 16–26.
[43] Z.Q. Zhang, J.L. Huang, L. Zhang, M. Sun, Y.C. Wang, Y. Lin, J. Zeng, Facile synthesis of Cu-Pd bimetallic multipods for application in cyclohexane oxidation, Nanotech. 25 (2014) 435602.
[44] M. Nowotny, L.N. Pedersen, U. Hanefeld, T. Maschmeyer, Increasing the ketone selectivity of the cobalt-catalyzed radical chain oxidation of cyclohexane, Chem. Eur. J. 8 (2002) 3724–3731.
[45] A.R. Kim, S. Ahn, T.U. Yoon, J.M. Notestein, O.K. Farha, Y.S. Bae, Fast cyclohexane oxidation under mild reaction conditions through a controlled creation of redox-active Fe(II/III) sites in a metal-organic framework, ChemCatChem 11 (2019) 1–8.